

**The Relation between Ion Temperature Anisotropy  
and Formation of Slow Shocks in Collisionless  
Magnetic Reconnection**

K. Higashimori<sup>1</sup> and M. Hoshino<sup>1</sup>

---

K. Higashimori, Department of Earth and Planetary Science, University of Tokyo, Science Building 1, Hongo, 7-3-1, Japan. (higashi@eps.s.u-tokyo.ac.jp)

M. Hoshino, Department of Earth and Planetary Science, University of Tokyo, Science Building 1, Hongo, 7-3-1, Japan. (hoshino@eps.s.u-tokyo.ac.jp)

<sup>1</sup> Department of Earth and Planetary  
Science, University of Tokyo, Tokyo, Japan.

**Abstract.** We perform a two-dimensional simulation by using an electromagnetic hybrid code to study the formation of slow-mode shocks in collisionless magnetic reconnection in low beta plasmas, and we focus on the relation between the formation of slow shocks and the ion temperature anisotropy enhanced at the shock downstream region. It is known that as magnetic reconnection develops, the parallel temperature along the magnetic field becomes large in association with the anisotropic PSBL (plasma sheet boundary layer) ion beams, and this temperature anisotropy has a tendency to suppress the formation of slow shocks. Based on our simulation result, we found that the slow shock formation is suppressed due to the large temperature anisotropy near the X-type region, but the ion temperature anisotropy relaxes with increasing the distance from the magnetic neutral point. As a result, two pairs of current structures, which are the strong evidence of dissipation of magnetic field in slow shocks, are formed at the distance  $|x| \geq 115 \lambda_i$  from the neutral point.

## 1. Introduction

In the Earth's magnetotail, magnetic reconnection plays an important role in the conversion of magnetic field energy in two lobes into kinetic and thermal energy of plasmas in a plasma sheet. Since *Petschek* [1964] proposed the necessity of pairs of slow-mode shocks attached to the diffusion region in magnetic reconnection in order to achieve its efficient energy conversion rate, many studies have been devoted to this model. As for numerical studies, many MHD simulations have confirmed the existence of slow shocks along the reconnection layer. Namely, slow-mode waves, propagating from the neutral point toward two lobes and along the outflow jets at one time, steepen and result in the steady state two pairs of slow shocks as is suggested by Petschek [*Sato and Hayashi*, 1979; *Scholer*, 1989; *Abe and Hoshino*, 2001]. In addition, observations of ISEE [*Feldman et al.*, 1985] and Geotail [*Saito et al.*, 1995; *Seon et al.*, 1995] satellites have shown the existence of such slow shocks in the Earth's magnetotail. Especially, *Saito et al.* [1995] showed that the variation in the ion temperature is much larger than the electron temperature variation across slow shocks. This suggests that the ion scale dissipation mechanism would be strongly related to the formation of slow shocks in collisionless plasmas.

Until now, however, there is no clear consensus on the formation of slow shocks in magnetic reconnection by both hybrid and full-particle simulations, even though the formation of slow shocks itself has been demonstrated by slow shock simulations without magnetic reconnection [*Omidi and Winske*, 1989; *Karimabadi*, 1995; *Omidi et al.*, 1995], and by a Riemann problem of slow shocks [*Fujimoto and Nakamura*, 1994; *Lin and Lee*, 1995; *Liu et al.*, 2011]. Attempts to investigate slow shocks in a large scale reconnection with

two-dimensional hybrid codes were first done by *Krauss-Varban and Omid* [1995]. They showed a fine structure of the reconnection layer where the fast plasma flow is generated. They concluded that these transition layers did not confirm the properties of the expected slow shocks, and mentioned that the reason for this is due to the fact that the ion dissipation scale is comparable to the thickness of the developing plasma sheet. *Lin and Swift* [1996] and *Lottermoser et al.* [1998] also performed large scale hybrid simulations to investigate slow shocks in magnetic reconnection. *Lin and Swift* [1996] suggested that the isotropic Rankine-Hugoniot (RH) jump conditions of slow shocks were better satisfied with increasing distance from the neutral point in the case of no-guide field reconnection. *Lottermoser et al.* [1998] also showed the slow shock-like discontinuities, and suggested that the downstream ions were not directly heated by slow shocks as was shown by *Lin and Swift* [1996] but heated by the stochastic motion of ions. They discussed that the thin current sheet formed after reconnection became turbulent and such turbulent structures caused stochastic motion of ions.

That being the case, what causes such a discrepancy of the formation of slow shocks between MHD [*Sato and Hayashi*, 1979] and kinetic treatments of plasmas? We suggest that an important kinetic modification in magnetic reconnection would be ion temperature anisotropy along reconnection layers. Observations by ISEE-3 and Geotail satellites in the Earth's magnetotail reported that the ion temperature parallel to the magnetic field ( $T_{i,\parallel}$ ) is higher than that perpendicular to the magnetic field ( $T_{i,\perp}$ ) at the downstream region of slow shocks [*Cowley et al.*, 1984; *Hoshino et al.*, 2000]. Such ion temperature anisotropy is known to be produced by two plasma components, i.e., the convecting cold lobe ions with the velocity  $\mathbf{V}_d = c\mathbf{E} \times \mathbf{B}/B^2$  and the PSBL (plasma sheet boundary layer)

ion beams which are accelerated and ejected from the diffusion region. Preceding studies for magnetic reconnection by kinetic simulations also support the fact that  $T_{i,\parallel}/T_{i,\perp} > 1$  at the downstream of discontinuities along the reconnection layer [*Hoshino et al.*, 1998; *Lottermoser et al.*, 1998]. On the other hand, theoretical studies about slow shocks with the one-dimensional RH relations suggest that conditions required to satisfy slow shock RH relations become restricted by the ion temperature anisotropy,  $T_{i,\parallel}/T_{i,\perp} > 1$ , in the downstream region [*Lyu and Kan*, 1986; *Karimabadi et al.*, 1995]. They showed that slow shock solutions in anisotropic plasmas are greatly affected by the downstream temperature anisotropy. If  $T_{i,\parallel}/T_{i,\perp} > 1$  in the downstream region, slow shock solutions can exist only for the limited upstream Mach number regime. This means that the enhancement of ion temperature anisotropy along the reconnection layer makes it harder for slow shocks to exist in magnetic reconnection. In this study, we focus on this point and perform kinetic simulations for magnetic reconnection. Then, the relation between such ion temperature anisotropy and formation of slow shocks in magnetic reconnection is discussed in accordance with anisotropic RH relations.

In the following sections, we will first refer to the simulation model; second, show results of the kinetic simulation for magnetic reconnection, and lastly discuss the nature of discontinuities formed along reconnection layers in detail.

## 2. Simulation Model

In our study, the two-dimensional electromagnetic hybrid code, in which ions are treated as particles while electrons as a mass-less fluid, is used to investigate the formation of slow shocks in magnetic reconnection. Algorithm of our hybrid code is based on the method of general predictor-corrector loops [*Harned*, 1982; *Winske and Leroy*, 1984]. Within our

simulation, basic equations are as follows:

$$m_i \frac{d\mathbf{v}_i}{dt} = q_i \left( \mathbf{E} + \frac{\mathbf{v}_i \times \mathbf{B}}{c} \right), \quad (1)$$

$$\frac{\partial \mathbf{B}}{\partial t} = -c \nabla \times \mathbf{E}, \quad (2)$$

$$\mathbf{E} = -\frac{1}{q_i n_i} \nabla p_e - \frac{1}{c} \mathbf{V}_e \times \mathbf{B} + \eta \mathbf{J}, \quad (3)$$

$$\mathbf{V}_e = \mathbf{V}_i - \frac{c}{4\pi e n_i} \nabla \times \mathbf{B}, \quad (4)$$

$$\mathbf{V}_i = \frac{\int_{-\infty}^{\infty} \mathbf{v}_i f_i(\mathbf{v}_i) d\mathbf{v}_i}{\int_{-\infty}^{\infty} f_i(\mathbf{v}_i) d\mathbf{v}_i}, \quad (5)$$

$$\frac{\partial p_e}{\partial t} + (\mathbf{V}_e \cdot \nabla) p_e + \gamma p_e (\nabla \cdot \mathbf{V}_e) - (\gamma - 1) \eta \mathbf{J}^2 = 0, \quad (6)$$

where  $f_i$  is the velocity distribution function of ions and a charge neutral condition,  $q_i n_i - e n_e = 0$ , is assumed.  $\gamma$  is the adiabatic index and set to be 5/3 in this paper. As for electrons, we assume that the electron gas is isotropic and both the electron heat flux and the viscosity stress tensor are neglected. In our simulation, various parameters are normalized by the parameters in the initial lobe (e.g.,  $n = n/n_0$ ,  $\mathbf{B} = \mathbf{B}/B_0$ , and  $\mathbf{V} = \mathbf{V}/V_{A0}$ , where  $n_0$ ,  $B_0$ , and  $V_{A0}$  are respectively the density, the magnetic field, and the Alfvén velocity in the initial lobe).

In addition, the spatial profile of the resistivity is given by

$$\eta(x, y) = \eta_0 + \eta_c \cosh^{-2} \left[ \left( \frac{x}{l_x} \right)^2 + \left( \frac{y}{l_y} \right)^2 \right], \quad (7)$$

where  $\eta_0$  is the background resistivity due to ion-electron interactions. Here, the background resistive length  $\lambda_{r0} \equiv \eta_0 c^2 / (4\pi V_{A0})$  is set to be  $10^{-4} \lambda_i$ , where  $\lambda_i$  is the ion inertial length in the initial lobe.  $\eta_c$  is the anomalous resistivity due to some instabilities in the diffusion region, e.g., the lower hybrid drift and the drift kink instabilities. This resistive term is assumed to be independent of time and its resistive length is equal to  $3.6 \times 10^{-2} \lambda_i$ .

98  $l_x$  and  $l_y$  are the characteristic lengths to determine the size of the anomalous (electron)  
99 diffusion region and are set to be  $l_x = 1.0 \lambda_i$  and  $l_y = 0.5 \lambda_i$ , respectively.

The whole size of the two-dimensional system is  $-342 \lambda_i \leq L_x \leq 342 \lambda_i$  and  $-32 \lambda_i \leq L_y \leq 96 \lambda_i$ . Grid intervals,  $\Delta_x$  and  $\Delta_y$ , are both equal to  $1/3 \lambda_i$ . Initially, a double Harris equilibrium is assumed and periodic boundary conditions in both  $x$ - and  $y$ -direction are imposed. The initial spatial profile of magnetic field is given as

$$\mathbf{B}(y) = B_0 \left[ \tanh \left( \frac{y}{\delta_y} \right) - \tanh \left( \frac{y - y'_c}{\delta_y} \right) - 1 \right] \mathbf{e}_x, \quad (8)$$

where  $y'_c = 64.0 \lambda_i$  and the half thickness of an initial current sheet,  $\delta_y$ , is set to be  $1.2 \lambda_i$ .

The density is given by

$$n(y) = n_0 + n_c \cosh^{-2} \left( \frac{y}{\delta_y} \right) + n_c \cosh^{-2} \left( \frac{y - y'_c}{\delta_y} \right). \quad (9)$$

100 The ratio of the density at the center of the initial current sheet to the background one,  
101 i.e.,  $n_c/n_0$ , is set to be 4. We assume the uniform electron temperature,  $T_e = 5 \times 10^{-3}$   
102 ( $\beta_{e,0} = 10^{-2}$  in the initial lobes). Ions consist of two components: The current sheet ions  
103 and the background ions. The current sheet ion temperature is set to be  $T_{i,c} = 0.12$ , which  
104 satisfies the relation,  $n_c(T_{i,c} + T_e) = B_0^2/(8\pi)$ . As for the background ion temperature,  
105 we assume  $T_{i,0} = 5 \times 10^{-4}$  ( $\beta_{i,0} = 10^{-3}$  in the initial lobes). Both the current sheet and  
106 the background ion temperatures are given isotropically. We initially input 160 super-  
107 particles per cell at the center of the current sheet (i.e., 32 super-particles per cell at two  
108 lobes).

### 3. Results

109 First we shall show the whole structure of reconnection, focusing on discontinuities  
110 formed along reconnection layers. Next, the nature of such discontinuities in kinetic plas-

mas are investigated in accordance with MHD Rankine-Hugoniot relations in anisotropic plasmas.

### Structure of reconnection layer:

In Figure 1, we show the whole structure of reconnection at time  $t = 415 \Omega_i^{-1}$ . Magnetic field lines continuously reconnect with each other at the center of the simulation box and two pairs of reconnection layers are formed. In the region  $|x| < 70 \lambda_i$ , ions experience Speiser-type trajectories [Speiser, 1965; Nakamura *et al.*, 1998] and form a thin current sheet whose half thickness is about an ion inertial length. In  $70 \lambda_i < |x| < 110 \lambda_i$ , the current structure becomes in some degree turbulent and its half thickness reaches about  $5 \lambda_i$ . Then, the current appears to be concentrated in the areas along the PSBL as is predicted by MHD simulations.

Figure 2 shows enlarged views of the reconnection layers at  $x < 0$ . From the top to the bottom, magnetic field lines, the out of plane magnetic field  $B_z$ , flow vectors, the mean ion temperature  $\langle T_i \rangle = (T_{i,\parallel} + 2T_{i,\perp})/3$ , and the ion temperature ratio  $T_{i,\parallel}/T_{i,\perp}$  are shown. Vertical red dashed lines separate two regions: Region 1 and Region 2 as indicated in Figure 2(b). In Region 1, the reconnection layer reaches almost steady state and its global structure does not change over time except for small scale turbulent structures. In Region 2, the reconnection jet encounters the preceding plasmoid and the plasma flows diverge. At this time, the region  $|x| < 150 \lambda_i$  is filled with plasmas which originate from two lobes.

As is seen in Figure 2(a), magnetic field lines begin to bend from  $x \sim -115 \lambda_i$  and pile up from  $x \sim -125 \lambda_i$ . The out of plane magnetic field,  $B_z$ , shows a clear quadrupole signature at  $-50 \lambda_i < x$  [Hesse and Winske, 1994; Nakamura *et al.*, 1998]. In  $-120 \lambda_i < x < -50 \lambda_i$ ,



the oscillations of  $B_z$  appear near the central plasma sheet (CPS) [Karimabadi *et al.*, 1999]. The outflow velocity at  $y = 0$  is  $\sim 0.7 V_{A0}$  in Region 1 and  $\sim 0.5 V_{A0}$  in Region 2. In the piled-up region ( $x < -125 \lambda_i$ ), ions are heated and the ion temperature anisotropy considerably decreases as is seen in Figure 2(d) and 2(e), while in  $-120 \lambda_i < x$  (Region 1) the ion temperature anisotropy remains high especially in the transition region (the region between upstream and downstream). The ratio  $T_{i,\parallel}/T_{i,\perp}$  is about 4–6 and in good agreement with Lin and Swift [1996] and Lottermoser *et al.* [1998].

Figures 3(a)–(c) show three different ion velocity distribution functions  $f(v_x, v_y)$  in the upstream, transition, and downstream regions, respectively. These ion velocity distribution functions are constructed by using super-particles within the white squares shown in Figure 2(e). In the upstream region, only cold lobe ions exist with the  $\mathbf{E} \times \mathbf{B}$  drift velocity  $V_y \simeq cE_z B_x / B^2 \simeq -0.15 V_{A0}$ . In the transition region, both cold lobe ions and PSBL beam ions exist. Characteristic speed of the PSBL beam ions is  $V_{\text{ibeam}} \sim 1.2 V_{A0}$ , and it is known that these PSBL ions are accelerated in and around the diffusion region [Hoshino *et al.*, 1998]. Here, note that the ion temperature evaluated from these two components in Figure 3(b) gives  $T_{i,\parallel} > T_{i,\perp}$  in the transition region. In the downstream region, ions are considerably heated, and the shifted-Maxwellian distribution with the outflow velocity  $V_x \simeq -0.7 V_{A0}$  is observed.

Next, to investigate fine structures along reconnection layers in more detail, Figures 4–6 respectively show the cross-sectional views of discontinuities at  $x = -88.3 \lambda_i$ ,  $-115.0 \lambda_i$  and  $-145.0 \lambda_i$  of Figure 2. (These locations are indicated by black arrows at the bottom of Figure 2(e).) The horizontal axes correspond to  $y$  axes of Figure 2, which are normal to the initial current layer. From the left top to the right bottom, the ion density, bulk velocities

$V_x$  and  $V_y$ , the total magnetic field strength,  $x$  and  $z$  components of the magnetic field, the current along the initial current, the ion temperature ratio  $T_{i,\parallel}/T_{i,\perp}$ , and the anisotropic parameter  $\epsilon \equiv 1 - (\beta_{\parallel} - \beta_{\perp})/2$  are shown, respectively. The anisotropic parameter  $\epsilon$  is useful to discuss the net effects of the temperature anisotropy. The vertical dash-dotted line stands for the boundary between the upstream and transition regions. The vertical dotted line stands for the boundary between the transition and downstream regions. The main judgmental standard points to determine these boundaries are the changes of both outflow and inflow bulk velocities. Note that the horizontal dashed lines shown in both  $T_{i,\parallel}/T_{i,\perp}$ - and  $\epsilon$ -plots stand for the isotropic temperature baselines.

At  $x = -88.3 \lambda_i$ , the current  $J_z$  concentrates in the CPS, even though slow shock-like discontinuities are formed along the reconnection layers. At  $x = -115 \lambda_i$ , the enhancement of  $J_z$  is seen around the transition region. Such bifurcated structures of the current indicate that most of the magnetic field energy is converted into kinetic and thermal energy of plasmas not in the CPS but near the transition regions. As for the magnetic field, the out of plane magnetic field  $B_z$  is confined to the transition region. The changes of the density, the bulk velocity, and the magnetic field also show the slow shocks-like behavior across these discontinuities. At  $x = -145 \lambda_i$ , a pair of current layers can be seen clearly. Note that the downstream of the pair of the current layers is the plasmoid, and that the inherent heating mechanism would be different from that in the quasi-steady state region (Region 1). In Region 2, since the radius of curvature of the magnetic field at the CPS becomes as large as the ion gyro-radius, the ion motion becomes stochastic and would contribute to the plasma heating [Büechner and Zelenyi, 1989; Lottermoser et al., 1998].

As is shown in Figures 4–6,  $T_{i,\parallel}$  is larger than  $T_{i,\perp}$  in the transition region. The ion temperature anisotropies are reduced across the transition region, but we can observe a finite ion temperature anisotropy in the downstream region for  $x = -88.3 \lambda_i$ . In the downstream region, since plasma betas are larger than those in the transition region, net anisotropic effects are significant and may affect the structure of discontinuities and the plasma instability. Also it should be noted from  $\epsilon$ -plots in Figures 4–6 that this net anisotropic effect of ions becomes large with decreasing the distance from the neutral point. In  $-100 \lambda_i < x$ , the downstream temperature anisotropy is large and the fire-hose unstable condition is often satisfied as is shown in the  $\epsilon$ -plot of Figure 4. (Note that the fire-hose unstable condition is  $p_{\parallel} - p_{\perp} > B^2/(4\pi)$ , i.e.,  $\epsilon < 0$ .) At  $x = -115 \lambda_i$  (Region 1) and at  $x = -145 \lambda_i$  (Region 2), the ion temperatures are almost isotropic. From the point of view of RH relations in anisotropic plasmas, such downstream temperature anisotropy is important to discuss the discontinuities [Lyu and Kan, 1986; Karimabadi et al., 1995]. This effect in magnetic reconnection is discussed in the following subsection in more detail.

### Comparison with RH relation in anisotropic plasmas:

We shall investigate the nature of these discontinuities formed along reconnection layers by using RH relations in anisotropic plasmas [Karimabadi et al., 1995]. The basic equations are as follows:

$$[\rho V_n]_2^1 = 0, \quad (10)$$

$$\left[ \rho V_n^2 + \bar{p} + \frac{1}{3} \left( \epsilon + \frac{1}{2} \right) \frac{|\mathbf{B}|^2}{4\pi} - \epsilon \frac{B_n^2}{4\pi} \right]_2^1 = 0, \quad (11)$$

$$\left[ \rho V_n V_t - \epsilon \frac{B_n B_t}{4\pi} \right]_2^1 = 0, \quad (12)$$

$$\left[ \rho V_n \left( V^2 + \frac{\gamma}{\gamma - 1} \frac{\bar{p}}{\rho} \right) + \frac{\epsilon + 2}{3} V_n \frac{|\mathbf{B}|^2}{4\pi} - \epsilon V_n \frac{B_n^2}{4\pi} - \epsilon V_t \frac{B_n B_t}{4\pi} \right]_2^1 = 0, \quad (13)$$

where the brackets represent  $[A]_2^1 = A_1 - A_2$  and the subscripts, 1 and 2, represent upstream and downstream, respectively.  $A_n$  and  $A_t$  respectively stand for the normal and tangential components of  $A$ . In above equations, the total pressure  $\bar{p} = (p_{\parallel} + 2p_{\perp})/3$  is introduced instead of using the double-adiabatic theory. (In more detail, see *Karimabadi et al.* [1995].)

It is known that the modified intermediate Mach number  $M_n \equiv V_n/(\sqrt{\epsilon}V_{An})$  is useful to discuss the above RH solution, where  $V_{An} = B_n/\sqrt{4\pi\rho}$  is the Alfvén velocity normal to the shock front [*Hau and Sonnerup*, 1989]. Then, the relation between the upstream modified intermediate Mach number  $M_{n1}$  and its downstream value  $M_{n2}$  are obtained, after some algebraic calculations, as follows:

$$\Lambda_a(\epsilon_2, \theta_1, M_{n2}^2) \cdot \epsilon_1^2 M_{n1}^4 + 2\Lambda_b(\epsilon_1, \epsilon_2, \theta_1, \beta_1, M_{n2}^2) \cdot \epsilon_1 M_{n1}^2 + \Lambda_c(\epsilon_1, \epsilon_2, \theta_1, \beta_1, M_{n2}^2) = 0, \quad (14)$$

where

$$\begin{aligned} \Lambda_a &= \frac{\gamma - 1}{\gamma} \cdot \frac{\xi_2}{\cos^2 \theta_1} - \xi_1 M_{n2}^2 \tan^2 \theta_1, \\ \Lambda_b &= \xi_2 \left[ \frac{\gamma - 1}{\gamma} \cdot \frac{2(1 - \epsilon_1)}{3 \cos^2 \theta_1} + \frac{\epsilon_1 \beta_1}{2 \cos^2 \theta_1} - \epsilon_2 M_{n2}^2 \right] + \epsilon_1 \xi_1 M_{n2}^2 \tan^2 \theta_1, \\ \Lambda_c &= M_{n2}^2 \left\{ \epsilon_2^2 \xi_2 \left[ \frac{\gamma + 1}{\gamma} M_{n2}^2 - \frac{\epsilon_1 \beta_1}{\epsilon_2 \cos^2 \theta_1} + \left( \frac{\epsilon_1}{\epsilon_2} - 1 \right) \right. \right. \\ &\quad \left. \left. + \frac{2}{3} \left( 1 - \frac{1}{\epsilon_2} \right) \left( \frac{2\gamma - 2}{\gamma} - \tan^2 \theta_1 \right) \right] - \epsilon_1^2 \xi_1 \tan^2 \theta_1 \right\}, \end{aligned}$$

and

$$\begin{aligned} \xi_1 &= \frac{\gamma - 1}{\gamma} \left( M_{n2}^2 - 2 + \frac{1}{\epsilon_2} \right) - \frac{1}{3\gamma} \left( 2 + \frac{1}{\epsilon_2} \right), \\ \xi_2 &= (M_{n2}^2 - 1)^2. \end{aligned}$$

$\theta_1$  is the angle between the shock normal and the upstream magnetic field line. So four parameters, i.e., anisotropic parameters in both upstream and downstream regions, an upstream shock angle, and an upstream plasma beta are necessary to determine above RH relations. These parameters are calculated from physical quantities obtained by our simulation and we can obtain the relation between the upstream and downstream Alfvén Mach numbers. Then, if one chooses a certain upstream Alfvén Mach number, one obtains corresponding downstream Alfvén Mach numbers. It should be noted that since plasma betas in two lobes are much smaller than unity, the upstream anisotropic parameter  $\epsilon_1$  is almost equivalent to unity as is shown in Figures 4–6.

In Figure 7 we show such parameters in magnetic reconnection. From the top to the bottom, boundaries separating the upstream, transition, and downstream regions in the  $x$ - $y$  plane, the inflow velocity, the upstream shock angle, and the downstream anisotropic parameter are shown, respectively. To eliminate the effects of initial current plasmas, we do not analyze the region  $x < -150 \lambda_i$ . In Figure 7(a), we choose error bars for boundaries so that changes of both  $V_x$  and  $V_y$  are within them. Error bars for  $\theta_1$ ,  $V_{n1}$ , and  $\epsilon_2$  stand for standard variations due to the averaging procedure for both upstream and downstream regions. In order to determine the upstream shock angle, we first evaluate the angle between the CPS, i.e.,  $y = 0$ , and a shock surface,  $\theta_{SC}$ , by the method of the least square fit. Then, using magnetic field data obtained by our simulation results, we calculate the angle between the CPS and the upstream magnetic field. Finally, we obtain the upstream shock angle  $\theta_1$ , and the upstream velocity normal to the shock front, i.e.,  $|V_{n1}| = |V_x| \sin \theta_{SC} + |V_y| \cos \theta_{SC}$ . As for the downstream anisotropic parameter,  $\epsilon_2$ , we

eliminated points whose standard variations are greater than 0.5, because of difficulties in identifying their shock downstream structures.

Since  $\theta_1$  varies over the range of  $\theta_1 \simeq 78^\circ\text{--}89^\circ$  and the average of inflow velocity  $\bar{V}_{n1}$  is nearly equal to 0.12 from Figures 7(b) and 7(c), we can suppose that the upstream Alfvén Mach number normal to the shock surface,  $M_{n1} \equiv V_n / (\sqrt{\epsilon_1} V_A \cos \theta_{Bn})$ , varies in the range  $M_{n1} \geq 0.58$  ( $M_{n1}^2 \geq 0.33$ ). As for the downstream anisotropic parameter,  $\epsilon_2$  increases with increasing the distance from the magnetic neutral point in Region 1, and  $\epsilon_2$  is nearly equal to unity everywhere in Region 2.

Now, we know  $\epsilon_2$ ,  $\theta_1$ , and  $M_{n1}$ . In addition, the upstream plasma betas are nearly equal to  $10^{-2}$  everywhere in the upstream region. Therefore, we can draw RH shock solution curves. Figure 8 shows such RH solutions in three cases:  $(\beta_1, \theta_1, \epsilon_2) = (10^{-2}, 84^\circ, 0.60)$ ,  $(10^{-2}, 84^\circ, 0.85)$ , and  $(10^{-2}, 84^\circ, 1.00)$ . Since there is no recognizable dependence of  $\theta_1$  on the nature of shock solution curves,  $\theta_1$  is supposed to be  $84^\circ$  here. The curves in the region where  $M_{n1} \leq 1.0$  correspond to slow shock solutions. As is shown in the earlier works [Lyu and Kan, 1986; Karimabadi et al., 1995], slow shock solutions are sensitive to the temperature anisotropy and the solution curves stretch as  $\epsilon_2$  becomes large. From this figure, one can find that if  $\epsilon_2$  is larger than 0.85, the minimum  $M_{n1}^2$  value obtained by our simulation, i.e.,  $M_{n1}^2 = 0.33$  ( $M_{n1}^2 \geq 0.33$ ), always has intersection points with the RH shock solution curve and slow shock solutions can exist over the range  $0.33 \leq M_{n1}^2 \leq 1.0$ . On the other hand in the case of  $\epsilon_2 < 0.85$ , the area, where slow shock solutions can exist, shrinks and it becomes harder for slow shocks to have their solutions with given Mach numbers.

Based on the above discussion, let us examine Figure 7(d) again. The horizontal dash-dotted line corresponds to  $\epsilon_2 = 0.85$ . In the region  $-115 \lambda_i < x$ , since  $\epsilon_2$  is smaller than 0.85, the range of upstream Alfvén Mach numbers where slow shocks can exist becomes narrower. While in the outer region  $x \leq -115 \lambda_i$ , the ion temperature anisotropy is small and  $\epsilon_2$  is nearly equal to unity. It enables slow shocks to exist stationarily in the calculated upstream Alfvén Mach numbers. The compression ratio  $\rho_2/\rho_1$  in such regions [simulation/theory (error %)] can be calculated as [1.9/2.5 (32 %)] at  $x \sim -115 \lambda_i$  (Region 1) with  $M_{n1} = 0.95$ ,  $\theta_1 = 82.8^\circ$ ,  $\beta_1 = 10^{-2}$ , and  $\epsilon_2 = 0.98$ , and [2.1/2.6 (24 %)] at  $x \sim -145 \lambda_i$  (Region 2) with  $M_{n1} = 1.0$ ,  $\theta_1 = 87.5^\circ$ ,  $\beta_1 = 10^{-2}$ , and  $\epsilon_2 = 0.95$ .

#### 4. Discussion and Conclusion

We have discussed the relation between the ion temperature anisotropy obtained by our two-dimensional kinetic simulation of magnetic reconnection and the formation of slow shocks in accordance with the RH relations. From the point of view of RH relations in anisotropic plasmas, the parameters to determine shock solutions are the upstream plasma beta  $\beta_1$  and shock angle  $\theta_1$ , the downstream ion temperature anisotropy  $\epsilon_2$ , and the upstream Alfvén Mach number  $M_{n1}$ . Among these four parameters,  $\beta_1$ ,  $\theta_1$ , and  $\epsilon_2$  have particularly an important influence on the nature of RH shock solution curves. We have evaluated the spatial profiles of these parameters in magnetic reconnection and discussed whether or not the discontinuities satisfy the conditions for slow shocks. In this study, it has been shown that the downstream ion temperature anisotropy along the reconnection layer decreases with increasing distance from the neutral point, and that a pair of current layers is formed in the region where plasmas are considerably isotropized ( $|x| \geq 115 \lambda_i$ ). This spatial distribution of the downstream ion temperature anisotropy is

strongly related to the formation of slow shocks, and the relaxation of the ion temperature anisotropy allows RH shock solutions in a broad range of upstream Alfvén Mach numbers in collisionless magnetic reconnection. Let us discuss the dependence of such parameters on the formation of slow shocks in magnetic reconnection in more detail.

First, we will refer to effects of downstream temperature anisotropy. Previous studies for the RH solutions in anisotropic plasmas suggest that the most important parameter for the RH relations is the downstream anisotropic parameter  $\epsilon_2$  [Lyu and Kan, 1986; Karimabadi *et al.*, 1995]. In collisionless magnetic reconnection, such temperature anisotropy is due to the PSBL beam ions, whose characteristic bulk velocity is about the lobe Alfvén velocity. Plasma mixing between cold lobe plasma, whose bulk velocity is about a tenth of the lobe Alfvén velocity, and PSBL ion beam components result in high temperature parallel to the magnetic field. Under these circumstances, the downstream anisotropic parameter  $\epsilon_2$  becomes smaller than unity. Here, we would emphasize that the generation mechanism of the ion temperature anisotropy in magnetic reconnection is quite different from that in the slow shocks without magnetic reconnection. In case of slow shocks without reconnection, incident ions and backstreaming ions from the shock downstream region are known to form the ion temperature anisotropy. On the other hand, in the case of slow shocks with magnetic reconnection, in addition to the backstreaming ions, PSBL ion beams accelerated around the diffusion region can contribute to the ion temperature anisotropy as well [Hoshino *et al.*, 1998]. Getting back to the diagram of  $M_{n2}^2$ - $M_{n1}^2$  plot discussed before, as  $\epsilon_2$  becomes small, the region where slow shock solutions exist shrinks. This is the main reason why slow shocks are hard to have their solutions near the diffusion region in magnetic reconnection.



In addition to the formation of such temperature anisotropy, a particular interest is why the relaxation of the ion temperature anisotropy occurs away from the diffusion region. In collisionless magnetic reconnection, the anisotropic PSBL ions can become thermalized by the Alfvénic waves generated by the ion-cyclotron beam instability, the ion/ion cyclotron instability [Winske and Leroy, 1984], and the EMIIC (electromagnetic ion/ion cyclotron) instability [Winske and Omid, 1990]. From observations in the Earth’s magnetotail, the existence of the ion cyclotron beam instability in the PSBL has been confirmed [Kawano *et al.*, 1994; Takada *et al.*, 2005]. Additionally, the fire-hose instability can take place in the reconnection exhaust [Karimabadi *et al.*, 1999; Liu *et al.*, 2011]. Our simulation results also support the fire-hose instability enhanced near the CPS. As shown in Figures 4–6, since the temperature anisotropic parameter  $\epsilon$  is greater than 0, the fire-hose instability is absent in the transition region. However, near the CPS, the condition  $\epsilon < 0$  for the fire-hose instability can be satisfied in  $-100 \lambda_i < x$ . We think that these instabilities may play an important role in the relaxation process of the downstream ion temperature anisotropy. As a result, Maxwellian-like distribution functions of ions are observed away from the neutral point. From the viewpoint of anisotropic RH relations, such relaxation of the downstream temperature anisotropy away from the diffusion region enables slow shocks to have their solutions in wider range of the upstream Alfvén Mach numbers.

We briefly refer to the upstream shock angle,  $\theta_1$ . From our simulation results,  $\theta_1$  is more or less in the range of  $78^\circ$ – $89^\circ$ . According to the anisotropic RH relations, such a variation obtained by our simulation does not result in a recognizable impact on the nature of solution curves. However, if  $\theta_1$  is smaller than  $78^\circ$  by keeping the inflow velocity of 0.12,

the upstream Alfvén Mach number becomes in the range of  $M_{n1} < 0.58$  ( $M_{n1}^2 < 0.33$ ) and the slow shock condition is not satisfied.

In this paper, we have shown the existence of slow shock discontinuities and the resultant current sheet profiles in both Regions 1 and 2, but the behavior of the downstream temperature anisotropies are different between two regions. The downstream ion temperature in Region 2 is nearly isotropic, while that in Region 1 is rather high even though the temperature anisotropy can be relaxed with increasing distance from the X-type neutral point. This behavior seems to be important for the satellite observation of the slow mode shock. So far the observational study of the slow shock detection in the Earth’s magnetotail assumed the isotropic temperature [*Saito et al.*, 1995; *Seon et al.*, 1995], but the RH study of the slow mode shock including the temperature anisotropy may distinguish the slow shock region between Regions 1 and 2.

In Region 1, we found the relaxation of the anisotropic temperature and the formation of the slow shock, but one might indicate that larger scale simulations would result in more isotropic plasma distribution in the slow shock region. In fact, we studied larger scale simulations, but we found that as time goes on, other magnetic islands are formed from the diffusion region, grow, and are ejected into the outflow region. As a result, the size of Region 1 cannot become larger than  $\sim 120 \lambda_i$ .

We obtained that the minimum distance for relaxation of the temperature anisotropy required for the formation of slow shock is about 115 times ion inertia length based on our two-dimensional hybrid simulation. However, some other processes that are not included in our simulation may quickly reduce the ion temperature anisotropy in a shorter spatial scale from the X-type neutral point. Such candidates might be the three dimensionality

(e.g., drift-mode instabilities), or the instabilities due to electron kinetic effects which cannot be considered in our hybrid model. Recently *Yin et al.* [2007] performed the oblique slow shocks by full-particle simulations, and discussed how electron kinetic effects are related to kinetic Alfvén waves and could alter the structure of slow shocks. These possibilities will be investigated in future works.

**Acknowledgments.** This work was supported by the editing assistance from the GCOE program. We thank Masaki Fujimoto, Lin-Ni Hau, Mariko Hirai, and Ryo Yoshitake for useful discussions. We would like to express our gratitude to the two referees for a number of useful comments to improve this paper.

## References

- Abe, S. A., and M. Hoshino (2001), Nonlinear evolution of plasmoid structure, *Earth, Planets, and Space*, *53*, 663–671.
- Büechner, J., and L. M. Zelenyi (1989), Regular and chaotic charged particle motion in magnetotail-like field reversals. I - Basic theory of trapped motion, *J. Geophys. Res.*, *94*, 11,821–11,842.
- Cowley, S. W. H., R. J. Hynds, G. Richardson, P. W. Daly, K.-P. Wenzel, J. A. Slavin, and B. T. Tsurutani (1984), Energetic ion regimes in the deep geomagnetic tail - ISEE-3, *Geophys. Res. Lett.*, *11*, 275–278.
- Feldman, W. C., D. N. Baker, S. J. Bame, J. Birn, J. T. Gosling, E. W. Hones, Jr., and S. J. Schwartz (1985), Slow-mode shocks - A semipermanent feature of the distant geomagnetic tail, *J. Geophys. Res.*, *90*, 233–240.
- Fujimoto, M., and M. Nakamura (1994), Acceleration of heavy ions in the magnetotail

reconnection layer, *Geophys. Res. Lett.*, *21*, 2955–2958.

Harned, D. S. (1982), Quasineutral hybrid simulation of macroscopic plasma phenomena, *Journal of Computational Physics*, *47*, 452–462.

Hau, L., and B. U. Ö. Sonnerup (1989), On the structure of resistive MHD intermediate shocks, *J. Geophys. Res.*, *94*, 6539–6551.

Hesse, M., and D. Winske (1994), Hybrid simulations of collisionless reconnection in current sheets, *J. Geophys. Res.*, *99*, 11,177–11,192.

Hoshino, M., T. Mukai, T. Yamamoto, and S. Kokubun (1998), Ion dynamics in magnetic reconnection: Comparison between numerical simulation and Geotail observations, *J. Geophys. Res.*, *103*, 4509–4530.

Hoshino, M., T. Mukai, I. Shinohara, Y. Saito, and S. Kokubun (2000), Slow shock downstream structure in the magnetotail, *J. Geophys. Res.*, *105*, 337–348.

Karimabadi, H. (1995), Steepening of Alfvén waves and its effect on the structure of slow shocks, *Geophys. Res. Lett.*, *22*, 2693–2696.

Karimabadi, H., D. Krauss-Varban, and N. Omidi (1995), Temperature anisotropy effects and the generation of anomalous slow shocks, *Geophys. Res. Lett.*, *22*, 2689–2692.

Karimabadi, H., D. Krauss-Varban, N. Omidi, and H. X. Vu (1999), Magnetic structure of the reconnection layer and core field generation in plasmoids, *J. Geophys. Res.*, *104*, 12,313–12,326.

Kawano, H., M. Fujimoto, T. Mukai, T. Yamamoto, T. Terasawa, Y. Saito, S. Machida, S. Kokubun, and A. Nishida (1994), Right-handed ion/ion resonant instability in the plasma sheet boundary layer: GEOTAIL observation in the distant tail, *Geophys. Res. Lett.*, *21*, 2887–2890.

- 389 Krauss-Varban, D., and N. Omidi (1995), Large-scale hybrid simulations of the magneto-  
390 tail during reconnection, *Geophys. Res. Lett.*, *22*, 3271–3274.
- 391 Lin, Y., and L. C. Lee (1995), Simulation study of the Riemann problem associated with  
392 the magnetotail reconnection, *J. Geophys. Res.*, *100*, 19,227–19,238.
- 393 Lin, Y., and D. W. Swift (1996), A two-dimensional hybrid simulation of the magnetotail  
394 reconnection layer, *J. Geophys. Res.*, *101*, 19,859–19,870.
- 395 Liu, Y.-H., J. F. Drake, and M. Swisdak (2011), The effects of strong tempera-  
396 ture anisotropy on the kinetic structure of collisionless slow shocks and reconnect-  
397 ion exhausts. I. Particle-in-cell simulations, *Physics of Plasmas*, *18*(6), 062,110, doi:  
398 10.1063/1.3601760.
- 399 Lottermoser, R., M. Scholer, and A. P. Matthews (1998), Ion kinetic effects in magnetic  
400 reconnection: Hybrid simulations, *J. Geophys. Res.*, *103*, 4547–4560.
- 401 Lyu, L. H., and J. R. Kan (1986), Shock jump conditions modified by pressure anisotropy  
402 and heat flux for earth’s bowshock, *J. Geophys. Res.*, *91*, 6771–6775.
- 403 Nakamura, M. S., M. Fujimoto, and K. Maezawa (1998), Ion dynamics and resultant  
404 velocity space distributions in the course of magnetotail reconnection, *J. Geophys. Res.*,  
405 *103*, 4531–4546.
- 406 Omidi, N., and D. Winske (1989), Structure of slow magnetosonic shocks in low beta  
407 plasmas, *Geophys. Res. Lett.*, *16*, 907–910.
- 408 Omidi, N., M. Johnson, D. Krauss-Varban, and H. Karimabadi (1995), Two-dimensional  
409 structure of slow shocks, *Geophys. Res. Lett.*, *22*, 299–302.
- 410 Petschek, H. E. (1964), Magnetic Field Annihilation, *NASA Special Publication*, *50*, 425.
- 411 Saito, Y., T. Mukai, T. Terasawa, A. Nishida, S. Machida, M. Hirahara, K. Maezawa,

- 412 S. Kokubun, and T. Yamamoto (1995), Slow-mode shocks in the magnetotail, *J. Geo-*  
 413 *phys. Res.*, *100*, 23,567–23,582.
- 414 Sato, T., and T. Hayashi (1979), Externally driven magnetic reconnection and a powerful  
 415 magnetic energy converter, *Physics of Fluids*, *22*, 1189–1202.
- 416 Scholer, M. (1989), Undriven magnetic reconnection in an isolated current sheet, *J. Geo-*  
 417 *phys. Res.*, *94*, 8805–8812.
- 418 Seon, J., L. A. Frank, W. R. Paterson, J. D. Scudder, F. V. Coroniti, S. Kokubun,  
 419 and T. Yamamoto (1995), Observations of a slow-mode shock at the lobe-plasma sheet  
 420 boundary in Earth’s distant magnetotail, *Geophys. Res. Lett.*, *22*, 2981–2984.
- 421 Speiser, T. W. (1965), Particle Trajectories in Model Current Sheets, 1, Analytical Solu-  
 422 tions, *J. Geophys. Res.*, *70*, 4219–4226.
- 423 Takada, T., K. Seki, M. Hirahara, T. Terasawa, M. Hoshino, and T. Mukai (2005), Two  
 424 types of PSBL ion beam observed by Geotail: Their relation to low frequency electro-  
 425 magnetic waves and cold ion energization, *Advances in Space Research*, *36*, 1883–1889,  
 426 doi:10.1016/j.asr.2003.09.075.
- 427 Winske, D., and M. M. Leroy (1984), Diffuse ions produced by electromagnetic ion beam  
 428 instabilities, *J. Geophys. Res.*, *89*, 2673–2688.
- 429 Winske, D., and N. Omid (1990), Electromagnetic ion/ion cyclotron instability at slow  
 430 shocks, *Geophys. Res. Lett.*, *17*, 2297–2300.
- 431 Yin, L., D. Winske, and W. Daughton (2007), Kinetic Alfvén waves and electron physics.  
 432 II. Oblique slow shocks, *Physics of Plasmas*, *14*(6), 062,105, doi:10.1063/1.2734951.

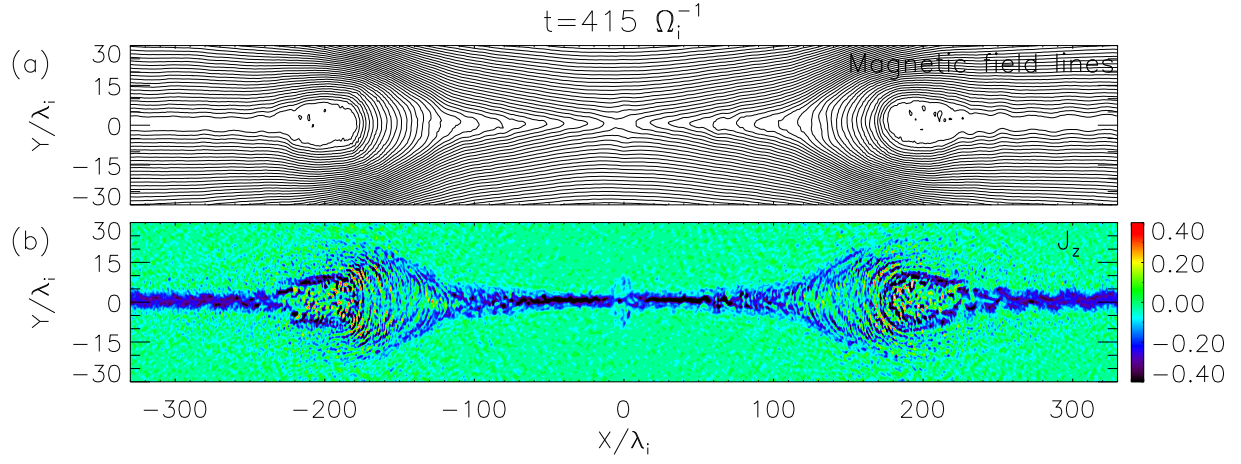


**Figure 1.** (a) Magnetic field lines and (b) the electric current in the  $z$  direction at time  $t = 415 \Omega_i^{-1}$ . The initial current is in the  $-z$  direction.

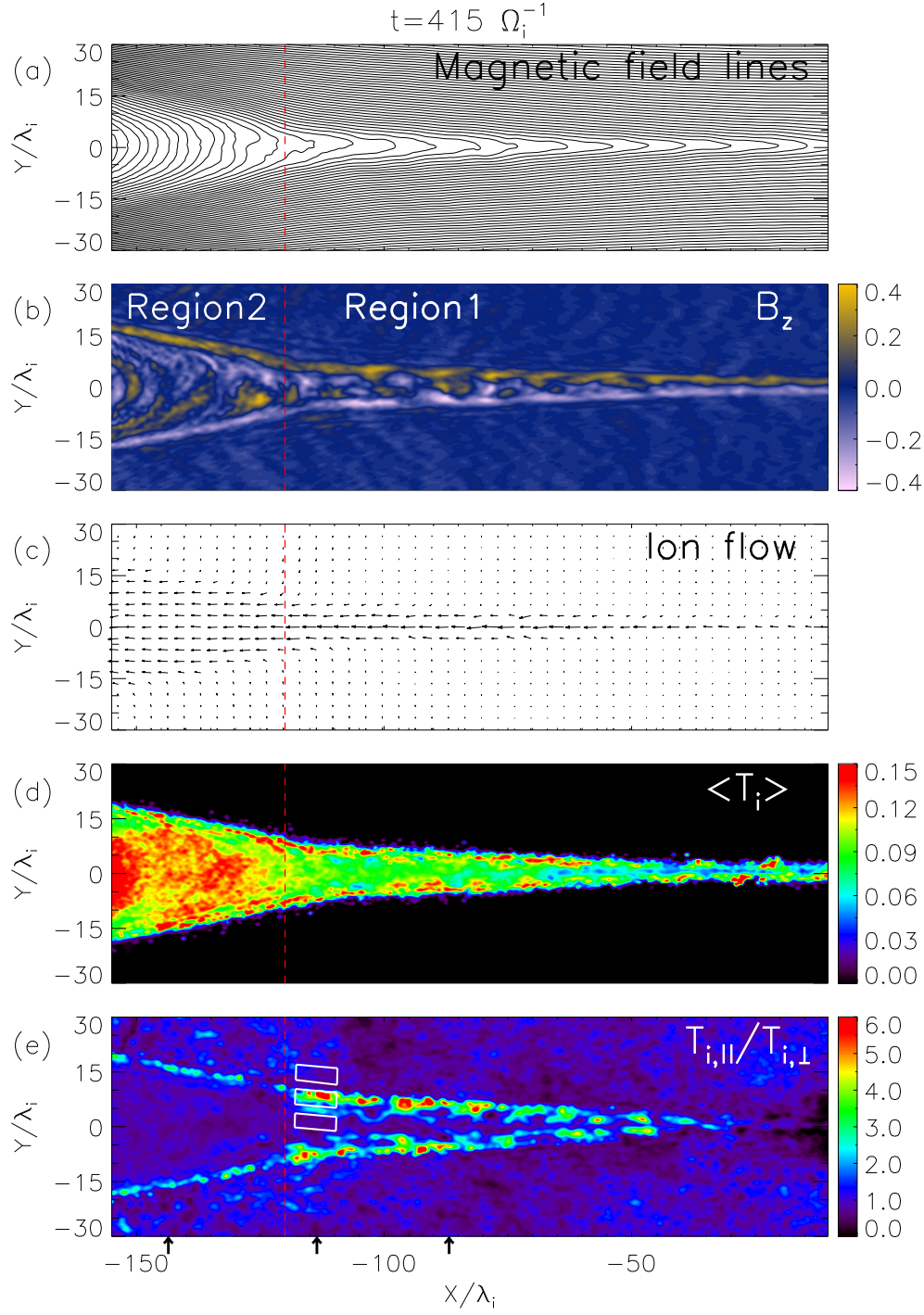


**Figure 2.** Enlarged views of the reconnection layer at  $x < 0$ . (a) Magnetic field lines, (b) the out of plane magnetic field  $B_z$ , (c) the ion flow vector, (d) the ion temperature, and (e) the ion temperature ratio  $T_{i,||}/T_{i,\perp}$  are shown in the  $x$ - $y$  plane.



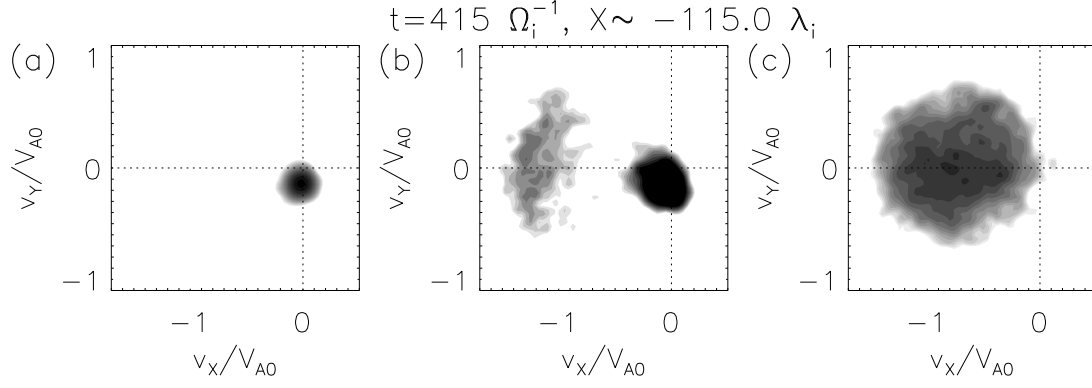


**Figure 3.** Ion velocity distribution functions ( $f(v_x, v_y)$ ) in the upstream, transition, and downstream regions. Their locations are indicated as white squares in Figure 2(e).

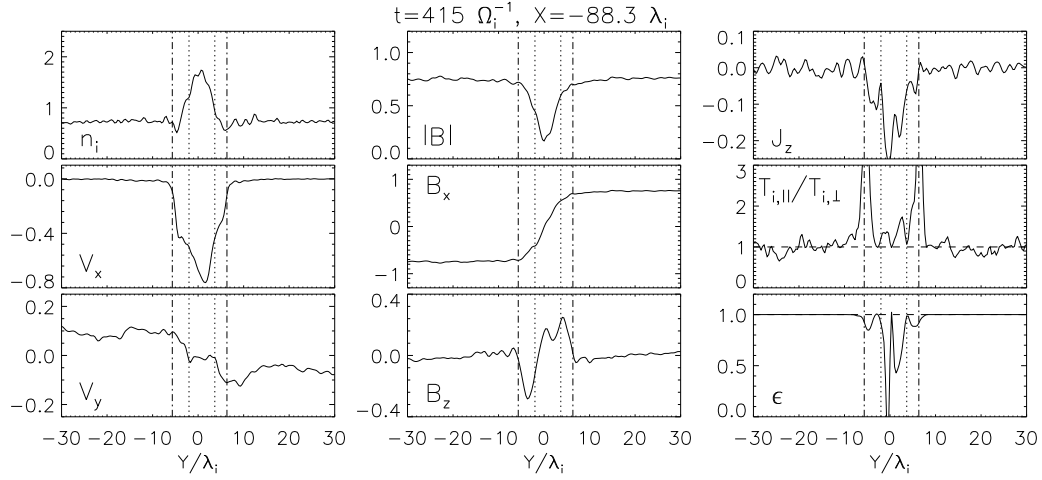


**Figure 4.** Cross-sectional views of discontinuities at  $x = -88.3 \lambda_i$ .

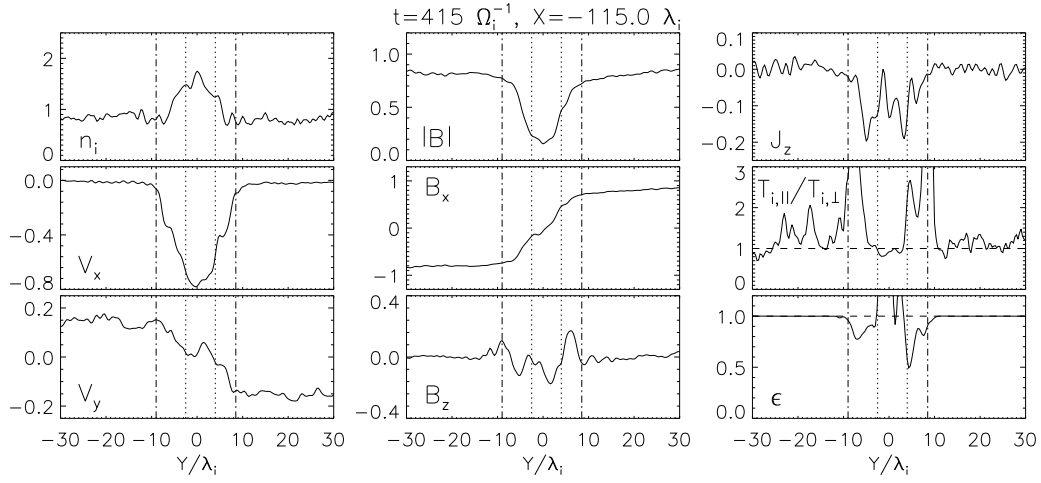


**Figure 5.** Cross-sectional views of discontinuities at  $x = -115.0 \lambda_i$ .

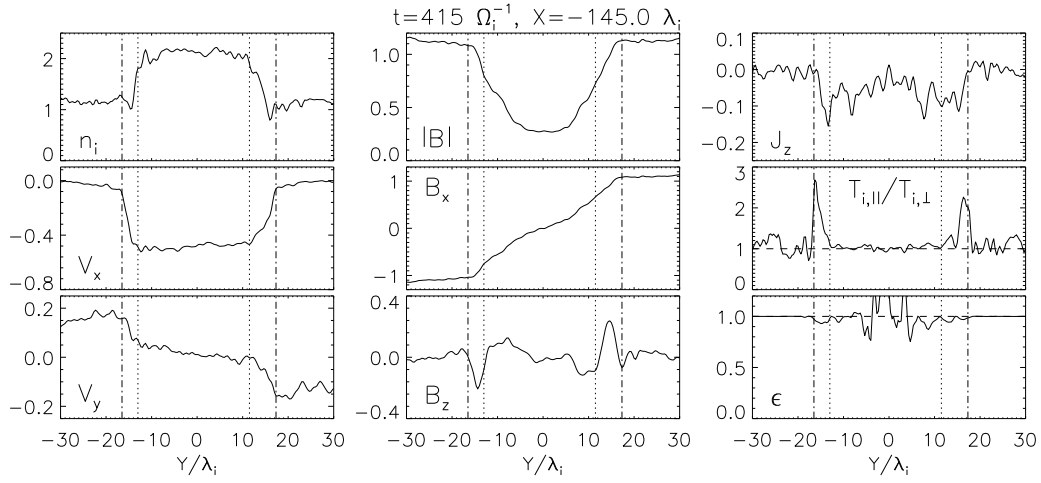


**Figure 6.** Cross-sectional views of discontinuities at  $x = -145.0 \lambda_i$ .

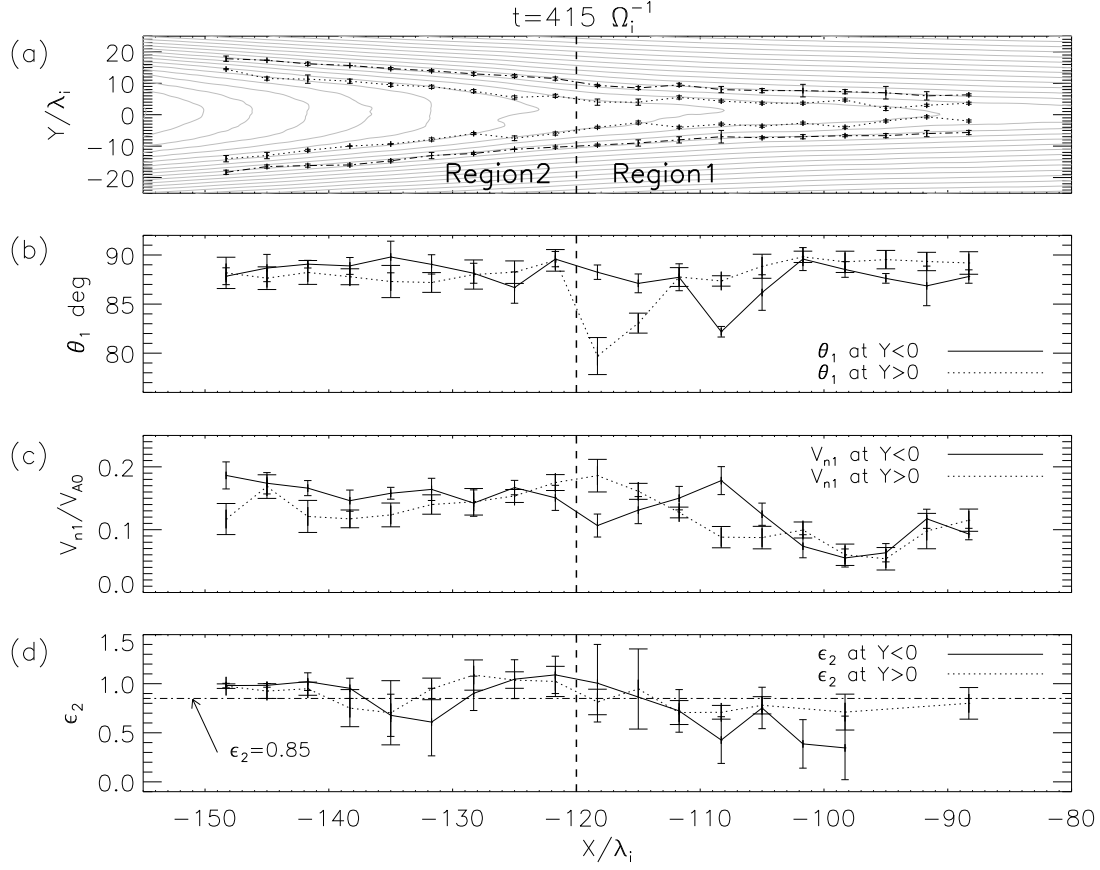


**Figure 7.** (a) Dash-dotted line and dotted line respectively stand for the boundaries separating the upstream and transient regions, and the ones separating the transient and downstream regions. In addition, spatial profiles of (b) the upstream shock angle, (c) the upstream velocity normal to the surfaces of discontinuities, and (d) the downstream anisotropic parameter are shown as a function of the distance from the neutral point.

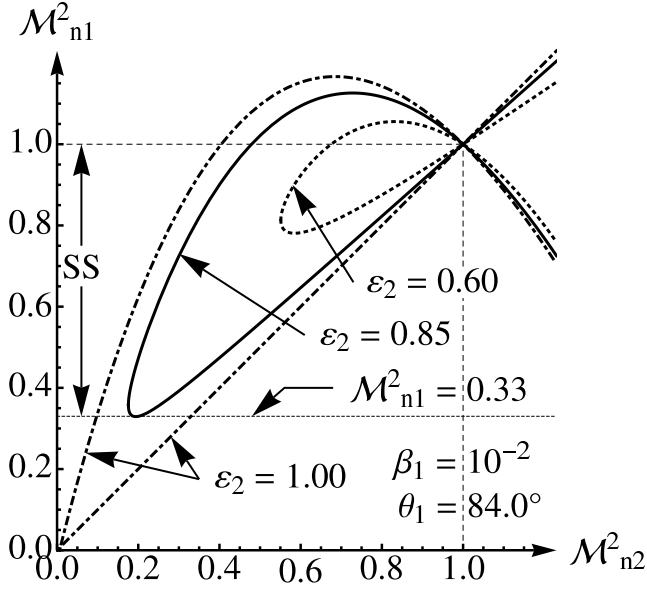


**Figure 8.**  $M_{n2}^2$ - $M_{n1}^2$  plot of RH solutions. Isotropic ( $\epsilon_2 = 1$ ) and anisotropic cases ( $\epsilon_2 = 0.85, 0.6$ ) are shown. The upstream plasma beta and the shock angle are assumed to be  $\beta_1 = 10^{-2}$  and  $\theta_1 = 84^\circ$  in all these three cases. **The** square of the minimum upstream Alfvén Mach number calculated in our simulation, i.e.,  $M_{n1}^2 = 0.33$ , **is** shown by the horizontal dotted line. The area where slow shocks (SS) can exist is indicated by a double-headed arrow ( $0.33 \leq M_{n1}^2 \leq 1.0$  in case of  $\epsilon_2 \geq 0.85$ ).